

CRYSTALLOGRAPHIC CONTROLS ON TRACE-ELEMENT INCORPORATION IN AURIFEROUS PYRITE FROM THE PASCUA EPITHERMAL HIGH-SULFIDATION DEPOSIT, CHILE-ARGENTINA

ANNICK CHOUINARD[§], JEANNE PAQUETTE AND ANTHONY E. WILLIAMS-JONES

Department of Earth and Planetary Sciences, McGill University, 3450 University Street, Montreal, Quebec H3A 2A7, Canada

ABSTRACT

The distribution of gold and other trace elements in the ore-stage pyrite from the high-sulfidation Au–Ag–Cu Pascua deposit in the El Indio belt in north-central Chile was studied using electron-microprobe and secondary-ion mass spectrometry (SIMS) imaging and analysis. The images show that concentrations of Au and Cu are concentrically zoned, and those of Ag, As, Se and Te are zoned both concentrically and sectorally. The principal trace-element associations are As–Ag, Au–Cu and Se–Te. We propose that the first two associations, As–Ag and Au–Cu, reflect coupled substitutions for Fe, whereas Te and Se replace S by direct-ion exchange. The near-identical patterns of sector zoning of Ag and As suggest that silver enters the structure of pyrite *via* a coupled substitution with As, in which one atom of Ag and one of As substitute for two Fe atoms, yielding $(\text{Ag}^{+}_{0.5}\text{As}^{3+}_{0.5})\text{S}_2$. Gold and copper were excluded during an interval in which growth conditions promoted the development of $|hk0|$ sectors at the expense of $|1111|$ sectors; their enrichment patterns show only slight evidence of sectoral preferences. With the analytical methods employed, we could not distinguish unequivocally between incorporation of gold as minute inclusions of the native metal or a coupled substitution of gold as an Au^{3+} ion and copper as a Cu^{+} ion for two Fe^{2+} ions, yielding $(\text{Au}^{3+}_{0.5}\text{Cu}^{+}_{0.5})\text{S}_2$. However, we favor the latter interpretation. Incorporation of gold as Au^{3+} is also consistent with evidence of unusually oxidizing conditions during the formation of the Pascua deposit. The zonation of invisible gold and associated trace elements in the ore-stage pyrite at Pascua is the first documented example of crystallographic structural control of the surface on the incorporation of multiple trace elements in pyrite. Moreover, the nature of this zonation provides clear evidence that incorporation of gold in pyrite does not necessarily involve coupled substitution with arsenic, as proposed for many other deposits. Not only can arsenic behave as a metal in the structure of pyrite, but its sectoral pattern of incorporation is a potentially sensitive indicator of redox conditions during mineralization.

Keywords: gold, copper, silver, arsenic, selenium, tellurium, pyrite, sector zoning, high sulfidation, element-distribution maps, electron-microprobe analysis, secondary-ion mass spectrometry, Pascua, Chile.

SOMMAIRE

La distribution de l'or et autres éléments traces dans la pyrite de la minéralisation principale du gisement épithermal à Au–Ag–Cu de Pascua, dans la ceinture de El Indio au centre-nord du Chili, a été étudiée par microsonde électronique et par spectrométrie de masse des ions secondaires. Les concentrations de Au et de Cu sont zonées concentriquement, alors que celles de Ag, As, Se et Te sont zonées concentriquement mais aussi en secteurs. Les associations principales des éléments-traces sont As–Ag, Au–Cu et Se–Te. Nous croyons que les deux premières, As–Ag et Au–Cu, sont le produit de substitutions couplées au site Fe, tandis que le Te et Se remplacent le S par échange direct d'anions. La zonation en secteurs presque identique de l'argent et de l'arsenic fait penser que l'argent est entré dans la structure de la pyrite *via* une substitution couplée avec l'arsenic, selon laquelle Ag et As remplacent deux atomes de Fe, donnant $(\text{Ag}^{+}_{0.5}\text{As}^{3+}_{0.5})\text{S}_2$. L'or et le cuivre ont été exclus durant un intervalle correspondant à des conditions de croissances favorisant le développement des secteurs $|hk0|$ aux dépens des secteurs $|1111|$. Ces deux éléments ne montrent qu'une très faible préférence pour certains secteurs. La méthode d'analyse utilisée ne nous permet pas de distinguer de façon non équivoque entre une incorporation de l'or sous forme de minuscules inclusions du métal ou celle de substitution couplée de l'or sous forme de Au^{3+} et du cuivre sous forme de Cu^{+} pour deux ions de Fe^{2+} , donnant $(\text{Au}^{3+}_{0.5}\text{Cu}^{+}_{0.5})\text{S}_2$. Cependant, nous préférons cette dernière interprétation. L'interprétation que l'or est présent sous sa forme Au^{3+} plutôt que Au^{+} concorde avec les indices de conditions très oxydantes durant la formation du gisement de Pascua. La zonation des éléments traces dans la pyrite de Pascua est le premier exemple documenté de contrôle crystallographique structural de la surface cristalline sur l'incorporation de multiples éléments traces dans la pyrite aurifère. De plus, la nature de la zonation met en évidence le fait que

[§] E-mail address: annick@geol.queensu.ca

l'or n'est pas nécessairement couplé avec l'arsenic, tel que plusieurs ont proposé à d'autres gisements de pyrite aurifère. Non seulement l'arsenic peut-il se comporter comme un métal dans la structure de la pyrite, mais sa zonation en secteurs pourrait potentiellement servir d'indicateur de conditions d'oxydo-réduction durant la minéralisation.

Mots-clés: or, cuivre, argent, arsenic, sélénium, tellurium, pyrite, zonation sectorielle, fort degré de sulfuration, carte de distribution des éléments, microsonde électronique, spectrométrie de masse des ions secondaires, Pascua, Chili.

INTRODUCTION

Gold is associated with trace elements such as Ag, As, Cu, Se and Te in the ore-stage pyrite of the high-sulfidation epithermal Pascua Au–Ag–Cu deposit, in northeastern Chile near the border with Argentina. The “invisible” gold in this pyrite accounts for approximately 50% of the ore reserves of the deposit (274 Mt of Au; Chouinard *et al.*, submitted). Evidence from scanning electron microscopy (SEM), electron-microprobe analysis and secondary-ion mass spectrometry (SIMS), presented here, suggests that the above elements are in solid solution within the pyrite, that their distribution is concentrically and sectorally zoned, and that their incorporation was controlled crystallographically by the nature of the growth surfaces. In contrast to most deposits studied thus far, gold at Pascua commonly displays an antithetic relationship with As, and it appears to have been incorporated *via* a coupled substitution with Cu. We seek here to explain the mechanism of incorporation of gold in pyrite from the Pascua deposit.

BACKGROUND INFORMATION

There is evidence that the incorporation of gold in pyrite is commonly associated with a substitution involving arsenic. The most widely held view is that substitution of As for S at the growth surface promotes substitution of Au (as Au⁺) for Fe (*e.g.*, Cabri *et al.* 2000, and references therein). However, Bostick & Fendorf (1999) challenged this view, and showed that As sorbed on pyrite is coordinated to sulfur atoms. Arehart *et al.* (1993) suggested that Au in arsenoan pyrite was probably incorporated as Au³⁺ at the Fe site through coupled substitution with As¹⁻ at the S site. Finally, Simon *et al.* (1999a) suggested, on the basis of XANES spectra and TEM imaging, that arsenoan pyrite may represent mixing of pyrite with fine layers of arsenopyrite or marcasite-type phases, and that the gold is structurally bound in the latter as Au⁺ and Au⁰.

Another important consideration is that models of trace-element incorporation in pyrite have been based on studies of samples from mineral deposits (sediment-hosted, mesothermal and volcanic-rock-hosted massive sulfide deposits) formed at near-neutral pH and relatively reducing $f(\text{O}_2)$ conditions. There has been very little attention paid to the trace-element content of pyrite deposited under the highly acidic and oxidizing conditions required to form high-sulfidation deposits. In

addition to economic considerations, the study of pyrite serves to improve our understanding of an important host for environmentally significant elements such as As and Se (*e.g.*, Hochella *et al.* 1999, Jambor *et al.* 2000, Savage *et al.* 2000, Bostick & Fendorf 2003).

GEOLOGY OF THE DEPOSIT

The Pascua high-sulfidation Au–Ag–Cu deposit, in northeastern Chile, and partially in Argentina, contains an estimated 225 million tonnes of ore with an average grade of 1.98 g/t Au and 66 g/t Ag (Barrick Gold Corporation, Annual Report, 2003). The Au–Ag mineralization occurred during the Miocene, and was hosted mainly by Triassic granitic rocks and by Miocene breccia bodies composed mainly of altered Triassic granitic rocks. Approximately 25% of the potentially economic reserves are hosted by Brecha Central, which is the most important hydrothermal breccia pipe on the property; it formed prior to mineralization.

The host rocks underwent two stages of high-sulfidation alteration, the latter of which was accompanied by main-stage Au–Ag–Cu mineralization. Early hydrothermal activity involved acidic condensates of magmatic vapors (with pH values probably as low as zero; Chouinard *et al.* 2005), and likely originated from a porphyry intrusion at depth on the Argentinian side of the deposit; these fluids produced extensive and pervasive advanced argillic alteration, local development of vuggy silica, and distal argillic to propylitic alteration. This alteration was locally followed by an intermediate, less acidic stage (possibly owing to an influx of meteoric water), which led to silicification and argillic and jarositic alteration, which was penecontemporaneous with the formation of Brecha Central. A renewal of highly acidic hydrothermal activity produced a second stage of intense advanced argillic alteration and vuggy silica, and subsequent Au–Ag–Cu mineralization.

The main stage of Au–Ag–Cu mineralization coincided with the termination of the second stage of alteration and involved precipitation of Au, either as the native metal or as a solid solution in the structure of pyrite and enargite. These metals are interpreted to have been transported by the magmatic vapors responsible for advanced argillic and vuggy silica and to have been deposited as a result of their cooling and subsequent condensation (Chouinard *et al.* 2005).

Main-stage pyrite occurs in all sulfide-rich parts of the deposit, and is distinguished from other types of pyrite by crystals containing anomalous and distinctly

zoned concentrations of Au, Ag, Cu, As, Te and Se. This pyrite is generally finer grained than other types of pyrite in the deposit, and locally may exhibit colloform banding, particularly at higher elevations. Its dull greenish luster and differential weathering arising from compositional heterogeneities facilitate its identification in the field.

Gold mineralization was followed by a sulfate stage of alteration, represented by barite and anglesite at lower elevations, and these minerals plus primary szomolnokite ($\text{FeSO}_4 \cdot \text{H}_2\text{O}$) at higher elevations. The main stage of mineralization was followed by a stage of silver enrichment in the upper parts of the deposit, represented by sulfide-poor, halogen-bearing Ag minerals such as iodargyrite and chlorargyrite. This stage produced a blanket containing these minerals above an elevation of ~4700 m, and represents the final phase of hydrothermal activity (Chouinard *et al.*, submitted). Supergene alteration is manifested by secondary jarosite and soluble sulfates (*e.g.*, coquimbite, voltaite and chalcantite), which formed as a result of sulfide oxidation (Chouinard 2003).

The present study is based on the two best pyrite crystals available, which are typical of the gold-bearing pyrite that formed during the main stage of Au-Ag-Cu mineralization. Both crystals are from rocks containing mainly quartz-pyrite-enargite and szomolnokite; one of them is subhedral and from level 4680 m, and the other is a colloform variant collected at an elevation of approximately 4800 m.

ANALYTICAL METHODS

Element-distribution maps and spot analyses were made using wavelength-dispersion spectrometry (WDS) and a JEOL JXA-8900L instrument at McGill University. Quantitative electron-probe micro-analyses (EPMA) were conducted at 20 kV, and a beam current of 40 nA. The following standards and analytical lines were employed: pyrite ($\text{FeK}\alpha$, $\text{SK}\alpha$), FeAsS ($\text{AsL}\alpha$), AuTe_2 ($\text{AuM}\alpha$, $\text{TeL}\alpha$), AgBiSe_2 ($\text{AgL}\alpha$, $\text{SeL}\alpha$), ZnS ($\text{ZnL}\alpha$) and CuFeS_2 ($\text{CuK}\alpha$). Peak and background were counted as follows: Fe (20 s), S (20 s), As (100 s), Au (200 s), Te (150 s), Ag (150 s), Se (150 s), Zn (100 s) and Cu (50 s). For elements not detected, means were calculated using half the detection limit.

Direct-ion images and quantitative secondary-ion mass spectrometry (SIMS) analyses were made at CANMET/MTL in Ottawa using procedures described in Cabri & McMahon (1995) and McMahon & Cabri (1998). Analyses were conducted using a Cameca IMS 4f instrument and a Cs^+ primary ion beam on carbon-coated polished thin sections of the two crystals. For quantitative analyses, the gold content was established with relative sensitivity factors (RSF) established from depth profiles on standards with known contents of gold. The minimum detection-limit for Au in pyrite is 0.04 g/t (40 ppb). Direct-ion images for all elements were

acquired from a multichannel plate with fluorescent screen using a Photometrics Series 200 CCD camera, and are 62.5 μm in diameter. During collection of each direct-ion SIMS image, the sample surface is sputtered by a primary ion beam. As such, because of repeated analyses, images may not be perfect replicas owing to slight degradation of the mineral's surface.

RESULTS

In the sample containing grains of subhedral pyrite, concentration of Au and Cu are restricted to two main concentric zones, whereas Ag, As, Se and Te are zonally distributed both concentrically and sectorally. The mean concentrations of As and Cu, determined by EPMA, are 0.08 and 0.24 wt%, respectively. The mean concentration of silver is 0.05 wt%, and it ranges from the detection limit (0.01 wt%) to 0.41 wt%. The concentration of Se is generally below the detection limit (0.01 wt%). Quantitative SIMS analyses of ore-stage pyrite yielded an average of 45.2 ppm Au for 20 analyses and a range from 0.2 to 386 ppm (Chouinard 2003). The sample of colloform pyrite contains more As and Ag; the mean values are 0.25 and 0.08 wt%, respectively. Gold concentrations are consistently high in colloform pyrite, averaging 84 ppm and ranging from 69 to 121 ppm (Chouinard 2003).

Figure 1 shows element-distribution maps in the subhedral crystal of pyrite (Table 1). During Stage II, the growth sectors were strikingly defined by their differential enrichment in As and Ag (Fig. 1) and, to a lesser extent, Se and Te. With the exception of the inner of the two main concentric zones, in which all elements were incorporated, zones with elevated Cu generally correspond to zones low in As and Ag, and *vice versa*; Se and, to a lesser extent, Te also are concentrated in the outer concentric zone. The four main stages, numbered from I to IV in Figure 1C, suggest at first glance an alternation of growth habits between cubic (Stage I and III) and octahedral (Stage II) sectors. We could not resolve the zoning pattern of Stage I. However, the striking pattern of sectoral enrichment seen in Stage II

TABLE 1. COMPOSITION OF THE PYRITE CRYSTAL FROM THE PASCUA DEPOSIT SHOWN IN FIGURE 1

Anal.	Fe	As	Zn	Au	S	Cu	Ag	Te	Se	Total
1	44.85	0.30	-	-	53.20	0.42	0.26	0.03	0.02	99.11
2	45.79	0.34	-	-	53.96	0.02	0.27	0.04	0.01	100.42
3	46.71	0.10	-	-	53.99	0.01	0.13	-	0.01	100.97
4	45.62	0.31	-	-	53.90	0.02	0.27	0.03	-	100.15
5	46.32	0.13	-	-	53.82	0.02	0.15	-	0.01	100.47
6	47.03	0.03	-	-	53.90	-	-	-	-	101.03
7	46.49	0.27	-	-	53.63	-	0.32	-	0.01	100.73
8	45.29	0.60	-	-	52.76	0.33	0.40	0.05	0.06	99.54

-: not detected. The compositional data are expressed in wt%. Detection limits (wt%): Fe 0.04, As 0.015, Zn 0.015, Au 0.03, S 0.023, Cu 0.018, Ag 0.015, Te 0.015, Se 0.015. The locations of the spots analyzed are shown in Figure 1C.

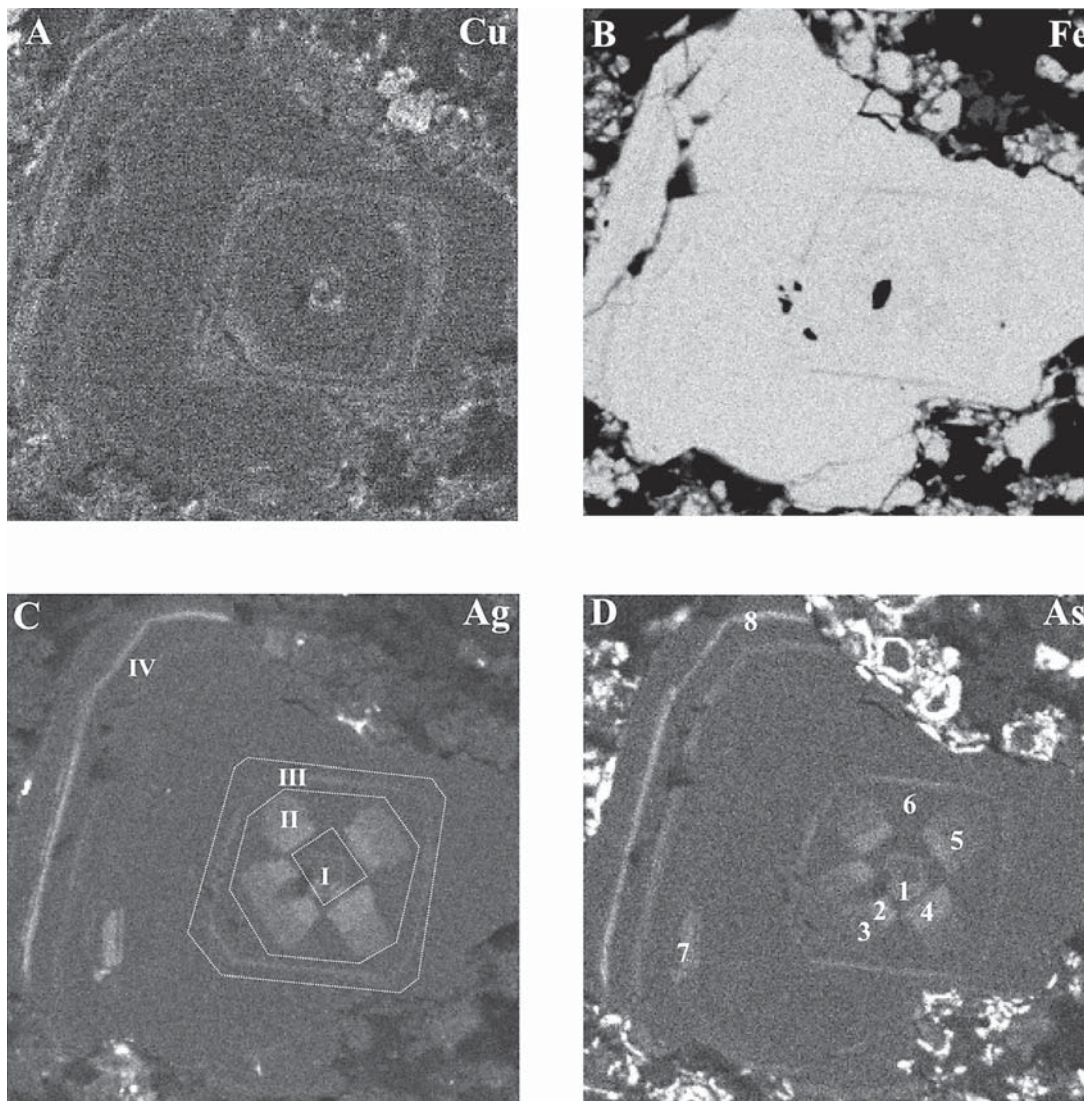


FIG. 1. X-ray (EMP) maps of A) Cu, B) Fe, C) Ag, and D) As in ore-stage pyrite from the Brecha Central area (4680 m elevation). The numbers in C indicate the various growth-zones described in the text, whereas numbers in D indicate locations of quantitative EMP spot-analyses, the results being presented in Table 1. The distribution of sulfur is not shown, but is very homogeneous. The bright spots on the Cu and As images are soluble sulfates, whereas the bright areas on the Ag image are due to late iodargyrite and chlorargyrite. The map dimensions are $275 \times 275 \mu\text{m}$. Direct-ion SIMS images of the core of this pyrite grain are presented in Figure 3.

of the subhedral pyrite at Pascua is best explained by a combination of $\{111\}$, $\{110\}$ and $\{hhl\}$ forms that was modeled with the SHAPE software (Dowty 1999; Fig. 2). The $\{hhl\}$ sectors could not be indexed precisely, but models of the wide concentric zones throughout Stage II suggest that $\{hhl\}$ faces are only slightly inclined relative to those of a (100) cube, and $\{113\}$ is

a reasonable approximation. Stage III coincides with a waning of the $\{110\}$ sectors and the appearance of the steeper $\{hhl\}$ faces. The growth-sector boundaries do not merge toward the center of the crystal, indicating that the section is slightly off-centered.

SIMS images of a section through the core of the crystal (Fig. 3) show relative enrichment patterns for

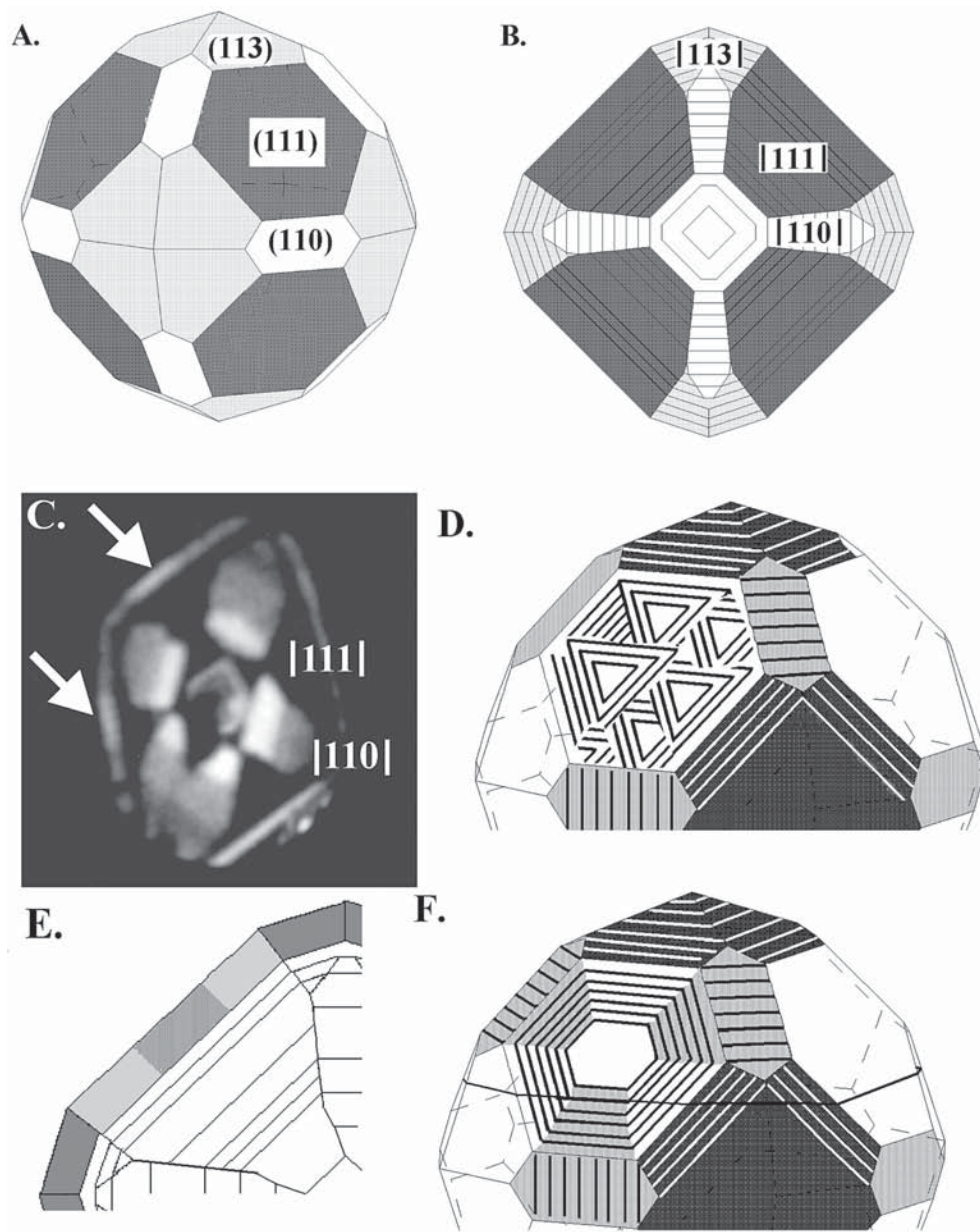


FIG. 2. Reconstruction of the zoning geometry using SHAPE (Dowty 1999). A. Sectoral zoning during Stage II is best explained by a growth morphology dominated by the $\{111\}$ octahedron having a low affinity for most trace elements. Trace elements were preferentially enriched in the sectors of a $\{110\}$ dodecahedron. A third form, tentatively indexed as $\{113\}$, explains the pinching out of the $\{110\}$ sectors prior to the impurity-rich concentric zone at the beginning of Stage III. B. Cross-section (slightly off-center) through the crystal shown in A. C. The discontinuous zoning (white arrows) in the outer, impurity-rich concentric zone (Stage III) of the SIMS map for As suggests that selective incorporation was sensitive to the orientation of the growth steps. D. Faces of the $\{111\}$ octahedron are normally covered with three-sided growth hillocks on which growth steps oblique to the isometric axes are related by symmetry. E. Prior to the beginning of Cu and Au incorporation, the change in the pattern of zoning suggests the waning of $\{110\}$ sectors. A more complex pattern of zoning developed within the $\{111\}$ sectors, suggesting the presence of non-equivalent vicinal faces. F. The zoning pattern is consistent with the presence of more complex growth hillocks, where new steps on opposite sides are unrelated by symmetry and could therefore display different affinities for trace elements.

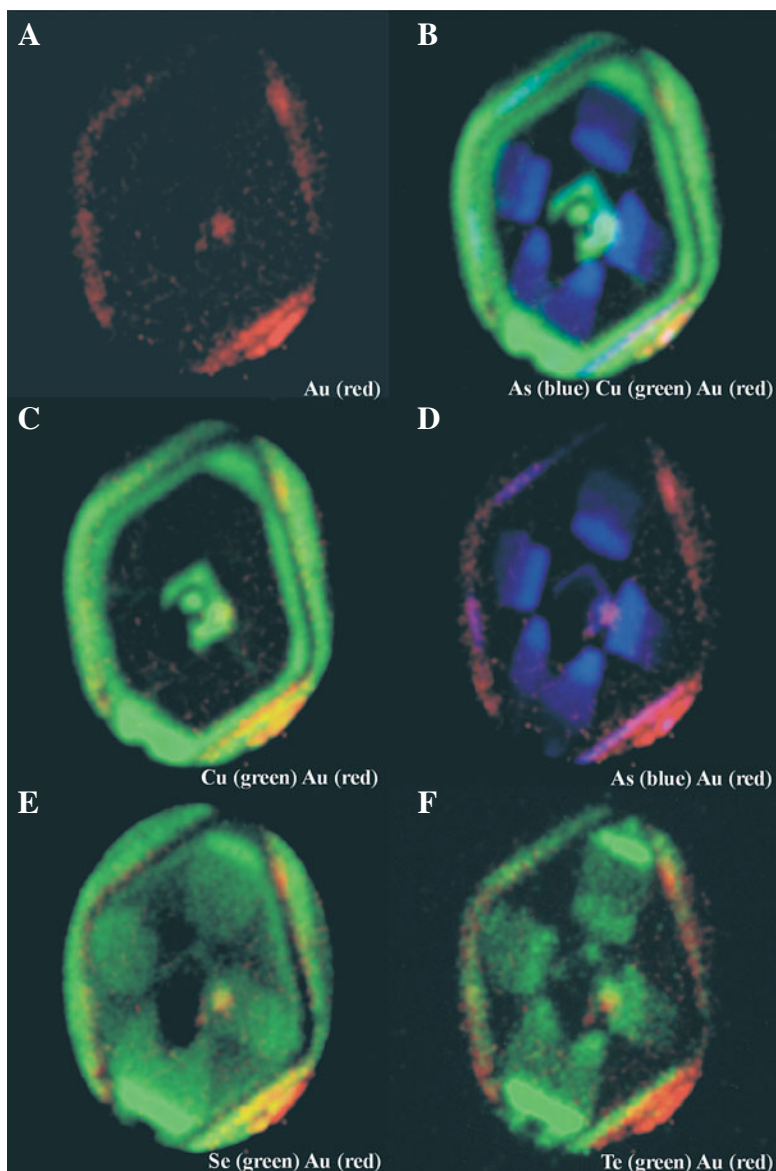


FIG. 3. Direct-ion SIMS images of A) Au, B) As–Cu–Au, C) Cu–Au, D) As–Au, E) Se–Au, and F) Te–Au of the core of the zoned crystal of pyrite shown in Figure 1. The dark area near the center of all images is a hole. The images show a positive correlation between concentrically zoned Au and Cu and, to a lesser extent, between Au and As, as well as between sectorally zoned Ag (from Fig. 1) and As. Note the clear affinity of Ag, As, Se and Te for the {111} octahedral sectors. The temporal trends of Te and Se from core to rim, within {111} sectors, are nearly exactly the opposite of those of As and Ag, which reach maximum incorporation near the center of the crystal. A combination of green and red will produce yellow, whereas blue and red will produce pink. The field of view is 62.5 μm and is entirely in pyrite.

Cu and As similar to those mapped with the electron microprobe. In addition, the SIMS images resolve the distribution patterns for Au, Te and Se, the concentrations of which are too low either to be detected or to provide interpretable patterns by electron-microprobe mapping. The distribution of Au and Cu defines sharp concentric zones (Stage I, and at the transition from Stage II to III). Within these zones, Au and Cu do not show the obvious sectoral preferences observed for other trace elements, such as Ag, As, Se and Te. Details of the Stages I and II of growth visible in electron-microprobe maps of Figure 1 are shown in the SIMS elemental maps of Figure 3. The exclusion of Au and Cu during Stage II is particularly noticeable. In contrast, Ag (Fig. 1C), As, Te and Se were incorporated throughout all stages, but they show specific sectoral preferences during Stage II, at which point all four elements were preferentially incorporated on $\{110\}$ rather than $\{111\}$ sectors. However, more subtle similarities are also noticeable for specific pairs of elements: within $\{110\}$ sectors, Ag (Fig. 1C) and As concentrations are highest at the beginning of Stage II, where the $\{111\}$ sectors first expanded, whereas Te and Se concentrations were highest toward the end of Stage II. The preference of selenium for the $\{111\}$ sectors over $\{110\}$ sectors is weaker than the differential sectoral incorporation displayed by Ag, As or Te. A slight deviation of the section from the (001) plane by $2-3^\circ$ easily accounts for the fact that the highest concentrations of Se and Te are restricted to a single opposing pair of $\{110\}$ sectors.

The colloform pyrite does not show obvious crystallographic faces, but SIMS images distinguish concentric bands, which provide evidence of temporal fluctuations of Cu, Au, As and Se incorporation (Fig. 4). No data are available for Ag and Te in this sample. A decrease in sulfur concentration in concentric zones generally corresponds to an increase in Se concentration. However, trace-element concentrations are too low to account for the significant depletion in S, which could be due to the uneven surface of pyrite, or to the presence of minor Fe-bearing soluble sulfates, which are common at Pascua. As in the subhedral Au-bearing pyrite, the distributions of Au and Cu, and to a lesser extent Se, are positively correlated (this statement refers only to zones interpreted to consist, exclusively or dominantly, of pyrite, on the basis of the high concentration of sulfur). Similarly, the enrichment patterns of As are mainly antithetic to those of Au and Cu, and overlap only slightly with the Au- and Cu-bearing concentric bands.

DISCUSSION

The presence of concentric and sector zoning in the subhedral pyrite suggests two different types of control on trace-element incorporation in pyrite. Concentric zoning records temporal changes and variations in conditions of pyrite precipitation (temperature or fluid

composition), whereas sectoral zoning indicates a stereochemical influence of the crystal-surface structure on the incorporation of trace elements.

Constraints on pyrite morphology and crystal-surface structure

Only three forms make up the majority of pyrite crystals: the cube $\{100\}$, the octahedron $\{111\}$ and the pyritohedron $\{210\}$. However, many more have been documented. Sunagawa (1957), in particular, noted the prevalence of $\{hk0\}$ forms in many Japanese hydrothermal replacement deposits.

Poisoning and enhancement of the $\{111\}$ face by As were documented in several Japanese deposits by Sunagawa & Takahashi (1955) and Hayashida & Muta (1952). Yet, despite interesting trends in pyrite habits within ore deposits, there has been very little experimental work on the controls of pyrite morphology. One notable contribution was that of Murowchick & Barnes (1987), who documented the effect of temperature and degree of supersaturation on hydrothermally grown pyrite between 250 and 500°C. They noted that increasing supersaturation induced by cooling promoted transitions in habit from the cube to octahedron, and speculated that other processes, including mixing with oxidizing groundwater, might induce similar changes in habit, if supersaturation increases as a result of oxidation of the sulfide species to form S_2^{2-} or HS_2^- .

Controls on the distribution of Se, Te, Ag and As

Stage II is characterized by strong differential partitioning of Ag, As and Te, which were preferentially incorporated on the $\{110\}$ faces and rejected by the $\{111\}$ faces. Sectoral zoning is less pronounced for selenium, which was incorporated on both types of sectors. Copper and gold were apparently excluded from the pyrite surfaces during this stage.

Two types of control are generally invoked to explain sectoral zoning. In the first type, differential growth-rates among non-equivalent forms have been documented as a controlling factor in the partitioning of trace elements (Burton *et al.* 1953, Hall 1953, Watson & Liang 1995). In the second type, well documented in minerals of the apatite group (Rakovan & Reeder 1994), in calcite (Paquette & Reeder 1995), in topaz (Northrup & Reeder 1994) and in fluorite (Bosze & Rakovan 2002), the role of surface structure on the differential incorporation of trace elements in a growing crystal has emerged as a major mechanistic control.

Pyrite has a halite-like structure, with iron ions arranged in a face-centered cubic lattice and alternating with a face-centered lattice of S_2 dimers. In other, simpler ionic cubic structures, such as halite, the higher tolerance of $\{111\}$ for impurity incorporation relative to $\{100\}$ faces is well documented, and the presence

of additives during crystal growth tends to promote the development of $\{111\}$ sectors at the expense of $\{100\}$ (Boistelle & Simon 1974). Investigations of the structure of the $\{100\}$ and $\{111\}$ pyrite surfaces by scanning tunneling microscopy confirm that these surfaces differ little from what would be expected from the bulk structure (Rosso *et al.* 1999). In their studies of the oxidation of the $\{100\}$ and $\{111\}$ surfaces of pyrite, Guèvremont *et al.* (1998) and Elsetinow *et al.* (2000) demonstrated that the latter are significantly more reactive than the $\{100\}$ faces. They suggested that alternating Fe-rich and S-rich outermost surfaces, which are a feature of the $\{111\}$ faces, could be responsible for their higher reactivity. If differences in surface structure influence reactivity, they could also be expected, to some degree, to result in differential incorporation of impurities among at least some nonequivalent growth-sectors of pyrite. However, the sectoral pattern suggests that the main control on differential incorporation may have been the specific orientation of growth steps, rather than overall differences in face structure. Throughout Stage II, the $\{111\}$ sectors that discriminated against Ag, As, Te and Se throughout Stage I and II are typically dominated by steps *oblique* to the isometric crystallographic axes. Incorporation was favored on $\{110\}$ faces, where growth occurs on steps *parallel* to the isometric crystallographic axes.

Sectoral zoning, less pronounced in Stage III than in Stage II, was characterized by increased overall trace-element enrichment. The abrupt reversal of these patterns of relative enrichment from Stage II to Stage III is consistent with a transition from $\{110\}$ growth sectors to $\{113\}$ sectors. The abrupt shift of growth-sector boundaries across concentric zones of Stage III suggests that the character of $\{111\}$ surfaces may have also changed substantially. The $\{111\}$ sector, usually dominated by triangular growth-hillocks, may well have broken down into two distinct sets of vicinal sectors, each dominated by steps that are parallel but unrelated by symmetry, with different preferences of trace-element incorporation (Fig. 2d). In diamond, similar patterns of nitrogen zoning are produced by growth on non-equivalent sets of steps on the $\{100\}$ and $\{111\}$ faces (Frank *et al.* 1990).

Natural As-rich pyrite can contain up to 8.4 wt% As, but the chemical state of the arsenic is not known with certainty (Arehart *et al.* 1993, Fleet *et al.* 1993, Mumin *et al.* 1994). Based on XANES spectra, Simon *et al.* (1999a) suggested that arsenic probably occurs in the As^- state, substituting for S and in a structural position similar to that in arsenopyrite. They also suggested that arsenic is possibly concentrated in submicrometric lamellae of marcasite or arsenopyrite within arsenoan pyrite. In light of the strong crystallographic selectivity on arsenic distribution and its coupled substitution with Ag in the Au-bearing pyrite at Pascua, we suggest that As is more likely to be incorporated as a cation substituting for Fe^{2+} . This interpretation is in agreement

with recent studies, including that of Helz *et al.* (1995), who suggested that thioarsenic species are important at low temperature and in sulfide-rich solutions, although the stoichiometry of the predominant species remains uncertain (Wood & Samson 1998). Bostick & Fendorf (1999, 2003) used data on X-ray absorption fine-structure spectroscopy (XAFS) and Raman spectroscopy obtained on pyrite surfaces to show that sorbed As is coordinated to S, and concluded that anion sorption of As to sulfide minerals may not be correctly modeled as simple ligand-exchange reactions.

The striking correlation of Ag and As, in their sectoral preferences, and their temporal variation within the octahedral sectors of Stage II, suggest that both ions entered the structure of pyrite as part of a coupled substitution. A charge-balanced scenario would be: $\text{Ag}^+ + \text{As}^{3+} \leftrightarrow 2\text{Fe}^{2+}$ yielding $(\text{Ag}^{+0.5}\text{As}^{3+0.5})\text{S}_2$. This substitution likely creates a distortion of the pyrite cell with $\text{Ag}^+ + \text{As}^{3+}$ having combined ionic radii of 201 pm (129 and 72 pm, respectively; Shannon 1976) compared to 150 pm (Shannon 1976) for the two iron ions replaced. Of the two impurities, the ionic radius of As^{3+} is the closer to the radius of Fe^{2+} . For this reason, we suggest that the As would be more easily incorporated in the crystal structure. The charge imbalance would then promote the coupled replacement of an adjacent Fe^{2+} ion by the larger silver ion.

Both Se and Te can readily replace S, but the radius of the selenide (232 pm) and telluride (250 pm) ions is substantially larger than that of the sulfide ion (219 pm; Huheey *et al.* 1993). Selenium and Te substitution for S would locally increase the unit-cell dimensions, possibly making the surface of pyrite locally more amenable to the incorporation of Au, Cu, As and Ag for Fe. During Stage II, the temporal trend of Se incorporation is exactly opposite to those of As and Ag, and the increase in Se at the transition between stages II and III correlates well with the increase in Cu, followed by Au incorporation. It is significant that Se, which shows the least evidence of temporal variation and only slight differential partitioning between $\{111\}$ and $\{hk0\}$ sectors, also shows the least misfit with S as an anionic species. Selenium is thus the most logical candidate of any of the trace elements for isomorphic substitution. Tellurium, which forms a sensibly larger anion, was incorporated in smaller amounts and was more efficiently excluded by $\{111\}$ than $\{hk0\}$ during Stage II.

Because of their narrow band-gap, reactions at the surface of semiconducting minerals are highly sensitive to the electronic structure of surface sites. It is overly simplistic to explain impurity incorporation in pyrite in terms of ionic radii, but the correlation of ionic size with relative trends of *sectoral* anionic substitution suggests the importance of surface site-configuration. Becker *et al.* (2001) recently emphasized the importance of step reactivity in adsorption and redox-reaction kinetics of semiconductors such as galena and pyrite. An important factor in impurity incorporation within the Pascua pyrite

may well have been the persistence of the strongly stepped $\{hh0\}$ and $\{hhl\}$ faces instead of the smoother faces of a $\{100\}$ cube or a $\{111\}$ octahedron. The presence of steps with different redox-reaction kinetics, coupled with the possibility of incorporating arsenic as a cation or anion, could modify the electronic structure of near-surface layers and profoundly influence the adsorption and eventual incorporation of other metallic cations.

Evidence from phase-stability relationships indicates that high-sulfidation deposits typically form in very oxidizing and acidic environments (Cooke & Simmons 2000). Such an environment appears to have been the case at Pascua, where alteration and mineralization assemblages are interpreted from phase equilibria to have formed at a $\log f(\text{O}_2)$ greater than -32 and a pH of around 0 (at 250°C ; Chouinard *et al.*, submitted). Hochella *et al.* (1999) noted that oxidation of $\{100\}$ pyrite surfaces observed by scanning tunneling microscopy is not random but proceeds in patches bounded dominantly by the $\langle 110 \rangle$ direction. The complex morphology of pyrite at Pascua and the preferential incorporation of elements such as Ag and As on specific sectors may therefore have been enhanced by step kinetics reflecting these unusually oxidizing conditions.

Controls on the distribution of Au and Cu

In the Au-bearing pyrite presented in Figure 3, gold and copper are restricted to two concentric zones (Stages I and III). Gold is distributed less evenly along these zones than copper. Neither gold nor copper displays the strong sectoral preference noted for Ag and As. These direct-ion SIMS images have a resolution of approximately one micrometer (G. McMahon, pers. commun., 2003), and therefore, do not allow us to clearly exclude the presence of scattered submicroscopic inclusions of native Au or other Au-bearing phases. Heasman *et al.* (2003) used EXAFS data to calculate the size of Au clusters in pyrite and determined a probable minimum size between 27 and 36 Å. On the other hand, Yang *et al.* (1998) used TEM images to document individual spheres of Au with an average size of $0.15\ \mu\text{m}$ on growth surfaces of pyrite. Their TEM images have a dark appearance and do not reveal the presence of gold clusters. Considering that gold and copper concentrations correlate very well, we suggest that most of the Au and Cu were incorporated directly into the structure of pyrite.

In contrast to most other documented occurrences of invisible gold in pyrite, at Pascua, the distribution of Au in ore-stage pyrite commonly correlates far better with Cu and Te than with As (*e.g.*, Cabri *et al.* 1989, Cook & Chryssoulis 1990, Arehart *et al.* 1993, Fleet *et al.* 1993, Fleet & Mumin 1997, Tarnocai *et al.* 1997, Yang *et al.* 1998, Simon *et al.* 1999a, b, Ashley *et al.* 2000, Cabri *et al.* 2000). Incorporation of Au during Stage III can be

divided into two substages. The first one is characterized by the incorporation of As along concentric zones, then by the incorporation of As and Au at the termination of the As zone. The second substage is characterized by the incorporation of both Au and Cu within a second concentric zone enriched in Cu. The association of Au and As is nearly absent in the colloform pyrite, in which Au shows a strong positive correlation with Cu. Thus, although there is locally a positive correlation between levels of Au and As, the strong positive correlation between concentrations of As and Ag, and of Au and Cu, are compelling evidence that, for the most part, Au and As were incorporated separately, *i.e.*, they were not linked in a coupled substitution. We therefore focus the remainder of this discussion on the Au-Cu association, rather than the well-known Au-As association, which has been explained satisfactorily by a coupled substitution in which As and Au replace S and Fe, respectively (reviewed above).

An important consideration in explaining the incorporation of Au is its size relative to the Fe^{2+} ion, which it must replace, and another is its charge. The atomic radius of Au^+ and of Au^{3+} is 151 and 99 pm, respectively, whereas that of Fe^{2+} is only 75. We propose that ionic size and charge constraints are satisfactorily met only if Au enters the pyrite structure as Au^{3+} in a coupled substitution with Cu^+ (91 pm) according to the coupled reaction Au^{3+} (99 pm) + Cu^+ (91 pm) \leftrightarrow 2Fe^{2+} (150 pm). Moreover, we note that the larger average size of the substituting cations is readily accounted for by substitution of Se^- (232 pm) for S^- (219 pm), which as noted earlier is the only ion to concentrate strongly with Au and Cu ions in the outer of the two main concentric zones. This interpretation is consistent with the low pH and high $f(\text{O}_2)$ associated with the formation of high-sulfidation deposits, which would have favored formation of Au^{3+} .

Although this hypothesis satisfactorily explains the incorporation of Au, it does not explain the fact that the concentration of Cu in the pyrite is appreciably higher than that of Au. It is therefore possible that some copper entered the structure of pyrite independently of gold. In principle, it could have been incorporated as Cu^{2+} by direct substitution for Fe^{2+} . However, available experimental data for both aqueous liquid and vapor suggest that copper in most ore-forming systems is transported as Cu^+ (Xiao *et al.* 1998, Archibald *et al.* 2002). Thus, if copper was incorporated separately from gold, it is unlikely to have entered the structure by simple substitution for Fe^{2+} but rather by a more complex path involving oxidation of Cu^+ . If this were the case for copper, it is also possible, as has been suggested by Maddox *et al.* (1998), that Au was incorporated into the structure by being adsorbed as a charged species (Au^{3+} or Au^+) that was subsequently reduced to Au^0 . This hypothesis does not, however, explain the strong correlation of Au with Cu and Se.

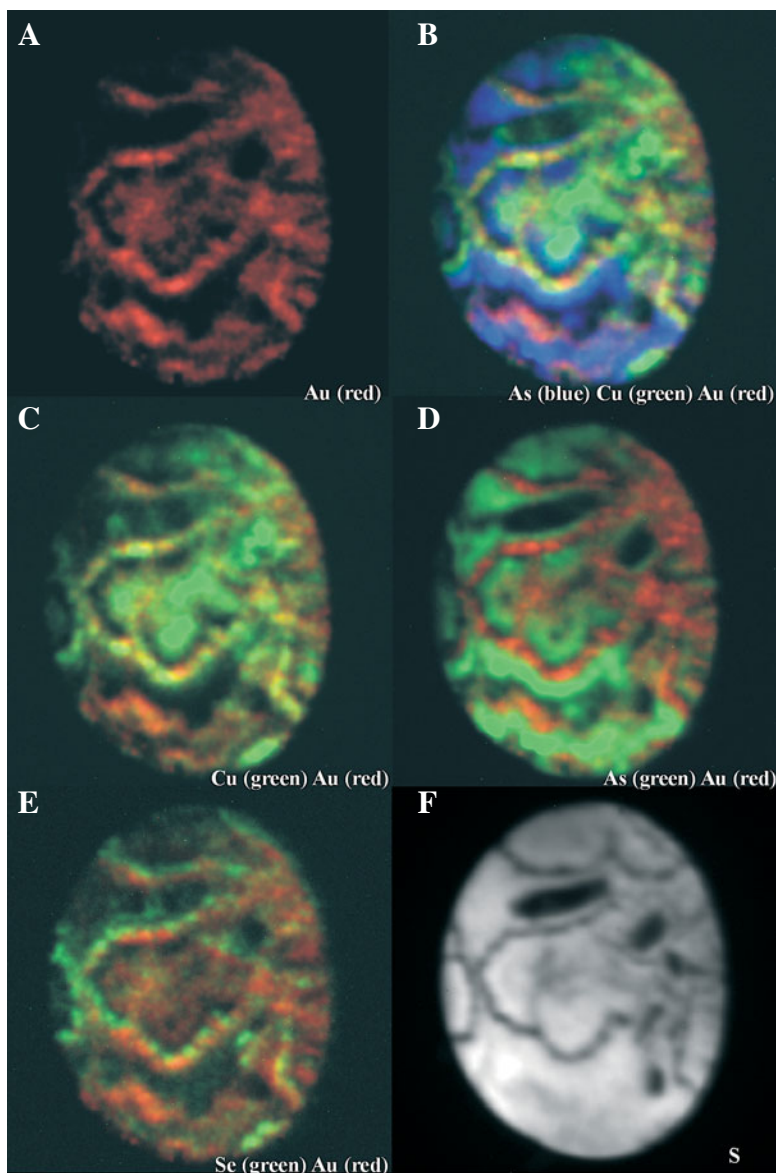


FIG. 4. Direct-ion SIMS images of A) Au, B) As–Cu–Au, C) Cu–Au, D) As–Au, E) Se–Au, and F) S in the colloform variant of the ore-stage pyrite. The dark ovoid areas in the S map probably reflect inclusions leached from the pyrite. A decrease in S corresponds to an increase in Se concentration in some of the growth bands, but also likely corresponds to the presence of Fe-bearing soluble sulfates. Elemental correlations are similar to those of the subhedral pyrite, *i.e.*, Au is mostly coupled with Cu, rather than As. A combination of green and red will produce yellow, whereas blue and red will produce pink. The field of view is 62.5 μm and is entirely pyrite.

We cannot resolve the exact morphology of the crystals during Stage I, which coincided with the earliest incorporation of Cu and Au. However, Stage III in subhedral pyrite shows an abrupt decrease in sectoral discrimination toward all the trace elements studied as well as an abrupt decrease in importance of the {110} sectors. This change in habit may reflect a change in bulk composition of the fluid, which could also have induced a significant change in the speciation of Cu and Au. Although the transport of gold to the surface of pyrite crystals depended mainly on the existence of stable species of Au³⁺, incorporation of this element in the structure of pyrite was controlled mainly by the surface reactivity of the mineral.

CONCLUSIONS

Back-scattered electron images, secondary ion images, and quantitative analyses show that Ag, As, Se and Te occur in solid solution in pyrite, and that their distribution was controlled crystallographically through selective incorporation, particularly on {hk0} surfaces. We demonstrate that: 1) gold shows only local correlation with As and has a stronger association with Cu and Se than with As; 2) arsenic is associated mainly with Ag and, to a lesser extent, Te; 3) selenium and Te are interpreted to have substituted by direct anion exchange with S, whereas Ag was incorporated through coupled substitution with As, in the form of (Ag⁺_{0.5}As³⁺_{0.5})S₂, and 4) where gold is associated with Cu, it likely entered the structure of pyrite through a coupled substitution, in the form of (Au³⁺_{0.5}Cu⁺_{0.5})S₂. This mechanism of Au incorporation differs significantly from that widely accepted, namely the coupled substitution of Au with As, in which the latter replaces S rather than Fe. The study of trace-element zoning in other morphologically complex pyrite could confirm whether the site selectivity of surface reactions is a dominant control on coupled substitutions in pyrite.

Our findings are the first to demonstrate the crystallographic control on the distribution of Ag, As, Te, and Se in pyrite from a high-sulfidation deposit. We also document a strong association between Au and Cu, and Ag with As in the structure of pyrite. Previous investigators have proposed that incorporation of Au (as Au⁺) in pyrite is controlled by substitution of As for S. The proposed coupled substitution of Au³⁺ with Cu⁺ in this study highlights the need for further investigations of the behavior of gold in acidic and highly oxidizing pyrite-depositing hydrothermal systems.

ACKNOWLEDGEMENTS

We are grateful to Barrick Gold Corporation and the staff at Compañía Minera Nevada for providing full access to the mine and samples. This research was conducted as part of a Ph.D. project funded by a NSERC scholarship to AC and research grants to

AEWJ by NSERC and Barrick Gold Corporation. Dr. Greg McMahon and Gilles Laflamme at CANMET provided valuable assistance on the technical aspects of SIMS analysis and imaging. The manuscript was improved significantly by constructive reviews from S. Chryssoulis and R.R. Seal II, and the suggestions of R.F. Martin.

REFERENCES

- ARCHIBALD, S.M., MIGDISOV, A.A. & WILLIAMS-JONES, A.E. (2002): An experimental study of the stability of Cu-chloride complexes in water vapor at elevated temperatures and pressures. *Geochim. Cosmochim. Acta* **66**, 1611-1619.
- AREHART, G.B., CHRYSOULIS, S.L. & KESLER, S.E. (1993): Gold and arsenic in iron sulfides from sediment-hosted disseminated gold deposits: implications for depositional processes. *Econ. Geol.* **88**, 171-185.
- ASHLEY, P.M., CREAGH, C.J. & RYAN, C.G. (2000): Invisible gold in ore and mineral concentrates from the Hillgrove gold-antimony deposits, NSW, Australia. *Mineral. Deposita* **35**, 285-301.
- BECKER, U., ROSSO, K.M. & HOCELLA, M.F. (2001): The proximity effect on semiconducting mineral surfaces: a new aspect of mineral surface reactivity and surface complexation theory? *Geochim. Cosmochim. Acta* **65**, 2641-2649.
- BOISTELLE, R. & SIMON, B. (1974): Epitaxies de CdCl₂, 2 NaCl, 3H₂O sur les faces (100), (110) et (111) des cristaux de chlorure de sodium. *J. Crystal Growth* **26**, 140-146.
- BOSTICK, B. C. & FENDORF, S. (1999): Arsenic sorption on metal sulfides. In Ninth Annual V.M. Goldschmidt Conf., Abstr. **7534**, LPI Contrib. 971, Lunar and Planetary Institute, Houston, Texas.
- _____ & _____ (2003): Arsenic sorption on troilite (FeS) and pyrite (FeS₂). *Geochim. Cosmochim. Acta* **67**, 909-921.
- BOSZE, S. & RAKOVAN, J. (2002): Surface-structure-controlled sectoral zoning of the rare earth elements in fluorite from Long Lake, New York, and Bingham, New Mexico, U.S.A. *Geochim. Cosmochim. Acta* **66**, 997-1009.
- BURTON, J.A., PRIM R.C. & SLICHTER, W.P. (1953): The distribution of solute in crystals grown from the melt. I. Theoretical. *J. Chem. Phys.* **21**, 1987-1991.
- CABRI, L.J., CHRYSOULIS, S.L., DE VILLIERS, J.P.R., LAFLAMME, J.H.G. & BUSECK, P.R. (1989): The nature of "invisible" gold in arsenopyrite. *Can. Mineral.* **27**, 353-362.
- _____ & MCMAHON, G. (1995): SIMS analysis of sulfide minerals for Pt and Au: methodology and relative sensitivity factors (RSF). *Can. Mineral.* **33**, 349-359.
- _____, NEWVILLE, M., GORDON, R.A., CROZIER, E.D., SUTTON, S.R., MCMAHON, G. & JIANG, DE-TONG (2000):

- Chemical speciation of gold in arsenopyrite. *Can. Mineral.* **38**, 1265-1281.
- CHOUINARD, A. (2003): *Alteration, Mineralization and Geochemistry of the High-Sulfidation Au–Ag–Cu Pascua Deposit, Chile–Argentina*. Ph.D. thesis, McGill Univ., Montreal, Canada.
- _____, WILLIAMS-JONES, A.E., LEONARDSON, R.W., HODGSON, C. J., SILVA, P., TÉLLEZ, C., VEGA, J. & ROJAS, F. (2005): Alteration and genesis of the multistage high-sulfidation Pascua Au–Ag–Cu deposit, Chile and Argentina. *Econ. Geol.* **100** (in press).
- COOK, N.J. & CHRYSOULIS, S.L. (1990): Concentrations of “invisible” gold in the common sulfides. *Can. Mineral.* **28**, 1-16.
- COOKE, D.R. & SIMMONS, S.F. (2000): Characteristics and genesis of epithermal gold deposits. In *Gold in 2000* (S.G. Hageman & P.E. Brown, eds.). *Rev. Econ. Geol.* **13**, 221-244.
- DOWTY, E. (1999): *Atoms 5.0: a Complete Program for Displaying Atomic Structures*. Shape Software, Kingsport, Tennessee 37663, USA.
- ELSETINOW, A.R., GUÈVREMONT, J.M., STRONGIN, D.R., SCHOONEN, M.A.A & STRONGIN, M. (2000): Oxidation of {100} and {111} surfaces of pyrite. Effects of preparation method. *Am. Mineral.* **85**, 623-626.
- FLEET, M.E., CHRYSOULIS, S.L., MACLEAN, P.J., DAVIDSON, R. & WEISNER, C.G. (1993): Arsenian pyrite from gold deposits: Au and As distribution investigated by SIMS and EMP, and color staining and surface oxidation by XPS and LIMS. *Can. Mineral.* **31**, 1-17.
- _____, & MUMIN, A.H. (1997): Gold-bearing arsenian pyrite and marcasite and arsenopyrite from Carlin Trend gold deposits and laboratory synthesis. *Am. Mineral.* **82**, 182-193.
- FRANK, F.C., LANG, A.R., EVANS, D.J.F., ROONEY, M.-L.T., SPEAR, P.M. & WELBOURN, C.M. (1990): Orientation-dependent nitrogen incorporation on vicinals on synthetic diamond cube growth surfaces. *J. Crystal Growth* **100**, 354-376.
- GUÈVREMONT, J.M., ELSETINOW, A.R., STRONGIN, D.R., BEBIE, J. & SCHOONEN, M.A.A (1998): Structure sensitivity of pyrite oxidation: comparison of the {100} and {111} planes. *Am. Mineral.* **83**, 1353-1356.
- HALL, R.N. (1953): Segregation of impurities during the growth of germanium and silicon crystals. *J. Phys. Chem.* **57**, 836-839.
- HAYASHIDA, S. & MUTA, K. (1952): Relation of trace-element content and crystal form in pyrite. *J. Mining Inst. Kyushu* **20**, 233-238 (in Japanese).
- HEASMAN, D.M., SHERMAN, D.M. & RAGNARSDOTTIR, K.V. (2003): The reduction of Au³⁺ by sulfide minerals and green rust phases. *Am. Mineral.* **88**, 725-738.
- HELZ, R.G., TOSSELL, J.A., CHARNOCK, J.M., PATTRICK, R.A.D., VAUGHAN, D.J. & GARNER, C.D. (1995): Oligomerization in As(III) sulfide solutions: theoretical constraints and spectroscopic evidence. *Geochim. Cosmochim. Acta* **59**, 4591-4604.
- HOCELLA, M.F., JR., MOORE, J.N., GOLLA, U. & PUTNIS, A. (1999): A TEM study of samples from acid mine drainage systems: metal – mineral association with implications for transport. *Geochim. Cosmochim. Acta* **63**, 3395-3406.
- HUHEEY, J.E., KEITER, E.A. & KEITER, R.L. (1993): *Inorganic Chemistry: Principles of Structure and Reactivity* (4th ed.). Harper Collins, New York, N.Y.
- JAMBOR, J.L., NORDSTROM, D.K. & ALPERS, C.N. (2000): Metal–sulfate salts from sulfide mineral oxidation. In *Sulfate Minerals – Crystallography, Geochemistry and Environmental Significance*, (C.N. Alpers, J.L. Jambor & D.K. Nordstrom, eds.). *Rev. Mineral. Geochem.* **40**, 303-350.
- MADDOX, L.M., BANCROFT, G.M., SCAINI, M.J. & LORIMER, J.W. (1998): Invisible gold: comparison of Au deposition on pyrite and arsenopyrite. *Am. Mineral.* **83**, 1240-1245.
- MCMAHON, G. & CABRI, L.J. (1998): The SIMS technique in ore mineralogy. In *Modern Approaches to Ore and Environmental Mineralogy* (L.J. Cabri & D.J. Vaughan, eds.). *Mineral. Assoc. Can., Short Course* **27**, 199-240.
- MUMIN, A.H., FLEET, M.E. & CHRYSOULIS, S.L. (1994): Gold mineralization in As-rich mesothermal gold ores of the Bogosu–Prestea mining district in the Ashanti gold belt, Ghana: remobilization of “invisible” gold. *Mineral. Deposita* **29**, 445-460.
- MUROWCHICK, J.B. & BARNES, H.L. (1987): Effects of temperature and degree of supersaturation on pyrite morphology. *Am. Mineral.* **72**, 1241-1250.
- NORTHROP, P.A. & REEDER, R.J. (1994): Evidence for the importance of growth-surface structure to trace element incorporation in topaz. *Am. Mineral.* **79**, 1167-1175.
- PAQUETTE, J. & REEDER, R.J. (1995): Relationship between surface structure, growth mechanism, and trace element incorporation in calcite. *Geochim. Cosmochim. Acta* **59**, 735-749.
- RAKOVAN, J. & REEDER, R.J. (1994): Differential incorporation of trace elements and dissymmetrization in apatite: the role of surface structure during growth. *Am. Mineral.* **79**, 892-903.
- ROSSO, K.M., BECKER, U. & HOCELLA, M.F., JR. (1999): Atomically resolved electronic structure of pyrite {100} surfaces: an experimental and theoretical investigation with implications for reactivity. *Am. Mineral.* **84**, 1535-1548.
- SAVAGE, K.S., TINGLE, T.N., O'DAY, P.A., WAYCHUNAS, G.A. & BIRD, D.K. (2000): Arsenic speciation in pyrite and secondary weathering phases, Mother Lode gold district, Tuolumne County, California. *Appl. Geochem.* **15**, 1219-1244.

- SHANNON, R.D. (1976): Revised effective ionic radii and systematic studies of interatomic distances in halides and chalcogenides. *Acta Crystallogr.* **A32**, 751-767.
- SIMON, G., HUANG, HUI, PENNER-HAHN, J.E., KESLER, S.E. & KAO, LI-SHUN (1999a): Oxidation state of gold and arsenic in gold-bearing arsenian pyrite. *Am. Mineral.* **84**, 1071-1079.
- _____, KESLER, S.E. & CHRYSOULIS, S. (1999b): Geochemistry and textures of gold-bearing arsenian pyrite, Twin Creeks, Nevada: implications for deposition of gold in Carlin-type deposits. *Econ. Geol.* **94**, 405-422.
- SUNAGAWA, I. (1957): Variation in the crystal habit of pyrite. *Geol. Surv. Japan, Rep.* **175**, 1-47.
- _____, & TAKAHASHI, K. (1955): Preliminary report on the relation between the *O*(111) face of the pyrite crystals and its minor contents of arsenic. *Geol. Soc. Japan, Bull.* **6**, 1-10.
- TARNOCAI, C.A., HATTORI, K. & CABRI, L.J. (1997): "Invisible" gold in sulfides from the Campbell mine, Red Lake greenstone belt, Ontario: evidence for mineralization during the peak of metamorphism. *Can. Mineral.* **35**, 805-815.
- WATSON, E.B. & LIANG, YAN (1995): A simple model for sector zoning in slowly-grown crystals: implications for growth rate and lattice diffusion, with emphasis on accessory minerals in crustal rocks. *Am. Mineral.* **80**, 1179-1187.
- WOOD, S.A. & SAMSON, I.M. (1998): Solubility of ore minerals and complexation of ore metals in hydrothermal solutions. In *Techniques of Hydrothermal Ore Deposits Geology* (J.P. Richards & P.B. Larson, eds.). *Rev. Econ. Geol.* **10**, 33-80.
- XIAO, Z., GAMMONS, C.H. & WILLIAMS-JONES, A.E. (1998): Experimental study of copper(I) chloride complexing in hydrothermal solutions at 40 to 300°C and saturated water vapor pressure. *Geochim. Cosmochim. Acta* **62**, 2949-2964.
- YANG, SIXUE, BLUM, N., RAHDERS, E. & ZHANG, ZHENRU (1998): The nature of invisible gold in sulfides from the Xiangi Au-Sb-W ore deposit in northwestern Hunan, People's Republic of China. *Can. Mineral.* **36**, 1361-1372.

Received November 28, 2003, revised manuscript accepted March 15, 2005.